Ship-based liquid water path estimates in marine stratocumulus

Paquita Zuidema

Rosenstiel School of Marine and Atmospheric Sciences, University of Miami, Miami, Florida, USA

Edgeworth R. Westwater

NOAA Environmental Technology Laboratory and Cooperative Institute for Research in Environmental Sciences, University of Colorado, Boulder, Colorado, USA

Chris Fairall and Duane Hazen

NOAA Environmental Technology Laboratory, Boulder, Colorado, USA

[1]   We examine liquid water paths (LWPs) derived from ship-based microwave radiometer brightness temperature (T_b) measurements collected within southeastern Pacific stratocumulus at 20°S, 85°W in October 2001. The boundary layer was typically well mixed and overcast. Three gaseous absorption models and two liquid dielectric models are evaluated. Total differences in retrieved LWP attributable to microwave absorption model differences are $10-25$ g m^{-2}, increasing with LWP. The most recent models produce the lowest LWPs. Most of the differences in the retrieved LWPs are caused by differences in the gaseous absorption models. Liquid dielectric model differences generate LWP differences of $\sim$6% of the total LWP. Radiosonde-calculated T_b using the most recent gaseous absorption model compare best to T_b measurements. The remaining LWP uncertainty due to model uncertainty is estimated at 6 g m^{-2}. The pre-1995 gaseous and liquid absorption models in combination produce LWPs that exceed the calculated adiabatic values. For the 6-day best estimate LWP time series, the clouds attained LWPs close to the theoretical adiabatic limit for LWPs up to 150 g m^{-2}, decreasing to $\sim$85% for LWPs of $\sim$250 g m^{-2}. Such deductions also depend upon how the cloud boundaries, to which the adiabatic calculation is sensitive, are determined. Light drizzle, as inferred from cloud radar reflectivitiy measurements, is common even at low LWPs, but heavy drizzle (radar reflectivities >0 dBZ, equivalent to a cloud base drizzle rate of $\sim$2 mm d^{-1}) is much less frequent, occurring <10% of the time even for LWPs of 200 g m^{-2}.

1. Introduction

[2]   Marine boundary layer clouds exert a strong radiative impact upon the global climate, ultimately accounting for a global-mean negative cloud radiative forcing [*Hartmann et al.*, 1992]. The cloud radiative impact is to first order determined by the liquid water path (LWP). The liquid water is radiatively integrally involved with the boundary layer cloud life cycle, through the longwave cloud top radiative cooling and liquid water's ability to absorb solar radiation. Liquid water paths also serve as important indicators of boundary layer cloud, aerosol, and precipitation process studies. For these reasons, observed LWPs are a common metric by which model simulations of boundary layer clouds are judged.

[3]   By far the best measure of LWP is provided by surface-based microwave radiometer (MWR) data. MWRs have the advantage of constant sampling at a temporal resolution of less than a minute, thereby providing greater detail on the LWPs than is available from satellite data. The LWP retrievals are more robust than those from space-based microwave measurements because of the easily modeled unpolarized cold space background. Examples of applications of the retrieved surface-based LWPs include microphysical retrievals [*Frisch et al.*, 1995; *Dong et al.*, 1998; *Frisch et al.*, 1998; *Löhnert et al.*, 2003], the quantification of cloud radiative impacts [*Fairall et al.*, 1990; *Cahalan et al.*, 1994; *Zuidema and Evans*, 1998], drizzle parameterizations [*Comstock et al.*, 2004], and the measurement of aerosol indirect effects

[*Feingold et al.*, 2003]. At least two studies use measured LWPs to reach the important conclusion that marine stratus cloud LWPs are often close to the theoretically calculated maximum adiabatic values [*Albrecht et al.*, 1990; *Bretherton et al.*, 2004].

[4] The wide application of surface-based MWR-derived LWPs underlines the value of characterizing them well. Much attention has been devoted within the past decade to the microwave radiative models used to convert the MWR brightness temperature measurements into the LWPs meaningful to the cloud physics community. The research has shown that impact of model differences upon the retrieved LWPs is not negligible; for example, differences in well-accepted gaseous absorption models can generate systematic biases in LWP of $15-30$ g m^{-2} [*Marchand et al.*, 2003]. Within Arctic clouds, the application of more recent clear air and cloud liquid models reduced original LWP estimates by $20-30\%$ [*Westwater et al.*, 2001]. Such a reduction in the estimated LWPs for low-latitude marine stratocumulus would have consequences for inferences about the adiabatic nature of stratocumulus LWPs, as well as for further deductions on stratocumulus climate impacts and processes.

[5] The continuing evolution in the radiative transfer theory describing microwave vapor absorption and emission has been aided by simultaneous improvements in the quality of radiosonde data. Radiosonde data can now establish a reliable benchmark against which to gauge microwave water vapor absorption models [e.g., *Mattioli et al.*, 2005]. One important recent result is that comparisons to high-quality sonde data demonstrate the post-1995 gaseous absorption models are more accurate than the pre-1995 models [*Mattioli et al.*, 2005].

[6] Liquid dielectric models are thought to be better known than the gaseous models [*Westwater et al.*, 2005] but are also more difficult to assess (than the gas models) because sondes do not measure liquid water. Validations have typically relied on aircraft data, [e.g., *Westwater et al.*, 2001; *Zuidema et al.*, 2005], which are expensive to collect and infrequently available, or radiative flux closure assessments [*McFarlane and Evans*, 2004; *Zuidema et al.*, 2005], which require extensive additional information. Marine stratocumulus with a well-mixed boundary layer provide the opportunity for another approach for evaluating the cloud liquid models, by comparing the retrieved LWPs against adiabatic values.

[7] To date, the impact of model improvements, both gaseous and liquid, upon LWPs retrieved within low-latitude marine stratus regions has received little attention. An opportunity to do so is afforded by data collected during the Eastern Pacific Investigation of Climate (EPIC) experiment, conducted in October 2001 within the southeastern Pacific stratus region [*Bretherton et al.*, 2004]. R/V *Ronald Brown* conducted a 3-week-long cruise, with 1 week spent stationary at 20°S, 85°W. The meteorology prevailing during the field experiment favored a relatively well-mixed boundary layer with overcast skies and few upper level clouds. Data from this field experiment have been used to validate a European Center for Medium Weather Forecasting model boundary layer scheme (M. Köhler, personal communication, 2005), to formulate a mixed

layer budget analysis [*Caldwell et al.*, 2005], and to construct a drizzle parameterization [*Comstock et al.*, 2004].

[8] Section 2 describes the two microwave radiometers present during EPIC and includes a discussion on the influence of instrument noise. Section 3 describes an evaluation of the gaseous absorption models. Section 4 discusses the LWP retrieval, compares the liquid dielectric models to each other and evaluates various (gas, liquid) model combinations, including comparing them to the theoretical adiabatic maximum. Section 5 presents a best estimate LWP time series for $16-22$ October. Section 6 examines the implications for cloud processes through comparisons to the adiabatic values and drizzle frequency (where the latter is inferred from cloud radar reflectivities), and section 7 presents a summary.

2. Data

[9] The Environmental Technology Laboratory (ETL) utilizes two microwave radiometers for its ship-based experiments, both of them present during EPIC. One has channels at 20.6, 31.65, and 90.0 GHz frequencies, corresponding to wavelengths of 1.46, 0.95 and 0.33 cm (referred to here as the "Hughes" radiometer). It has been in use at ETL since 1987 [*Albrecht et al.*, 1990; *Fairall et al.*, 1990]. The other radiometer served as a prototype for those currently present at the Atmospheric Radiation Measurement (ARM) sites, with channels at 23.8 and 31.4 GHz (referred to here as the "mailbox" radiometer). It has been in use at ETL since approximately 1992.

[10] Ship motion is accounted for: pitch and roll movement is measured and their values are combined to obtain a pointing error correction, which is then applied to the MWR scan angle to correct back to either the vertically pointing values or a particular air mass value (for the calibration procedure). This is done with both radiometers. The ETL mailbox radiometer uses different software than the ARM mailbox MWRs and each instrument has slight differences, so that conclusions drawn about the ETL mailbox radiometer should not be inferred to apply to the ARM mailbox MWRs.

[11] A characteristic of MWRs is that their signal is amplified to aid in the signal's detection. This means that variations in the gain of a system caused by, for example, changes in supply voltages and the ambient temperature, have a big impact on the output voltages and thereby the brightness temperatures (T_b). If the instrument contributions are not considered explicitly, it is difficult to confidently differentiate the true cloud LWP variability from that caused by instrument electronic shifts. For the Hughes MWR, the system gain can be easily calculated from its preserved internal housekeeping data. This includes both large systematic changes in the system gain, and the ever-present random small-scale variations (i.e., instrument noise). This exercise is not possible with the mailbox MWR because one of the two required calibration parameters is determined by a tipping curve calibration [see *Han and Westwater*, 2000]. As shown in section 2.3, the mailbox tipping curve calibrations did not perform well during EPIC. For this reason, the Hughes MWR is used to evaluate the mailbox MWR
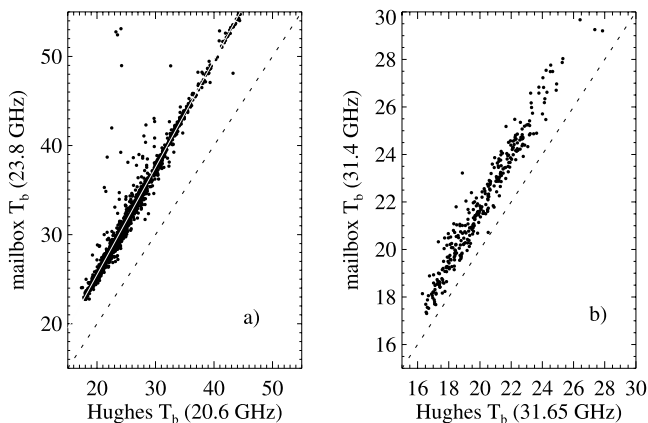
Figure 1. (a) Mailbox 23.8 GHz T_b versus Hughes 20.6 GHz T_b, for 11–16 October 1200 UTC and 19–24 October. The best fit line is shown by white line. (b) Mailbox 31.4 GHz T_b versus Hughes 31.65 GHz T_b, for 15–16 October 1200 UTC and 19 October. Data lying 1 K outside the best fit line shown in Figure 1a have been removed.

brightness temperature measurements, and to establish the LWP error bars caused by instrument noise.

2.1. Hughes Radiometer

[12] The Hughes radiometer equation is presented to elucidate how instrument variations contribute to the T_b and thereby the LWPs (but not that of the mailbox MWR, whose instrument noise variations we do not consider). The radiometer equation that relates the Hughes instrument observations to a physical atmospheric brightness temperature, slightly simplified, is given by [*Decker and Schroeder*, 1991]

$$T_b = CF * G * (V_m - V_r) + T_r \qquad (1)$$

where T_b is the atmospheric brightness temperature in units of K, CF is a calibration factor, G is the system gain in units of K counts^{-1}, V_m and V_r are the antenna and reference blackbody target voltages in units of counts, and T_r is the reference blackbody temperature. The system gain G is given by $(T_h - T_r)/(V_h - V_r)$, where T_h and V_h are the hot reference temperatures and voltages.

[13] The calibration factor CF accounts for waveguide losses and more generally for radiometer equation assumptions implicit in equation (1). A tipping curve calibration establishes the value of this coefficient when the radiometer scans a horizontally homogeneous (i.e., clear) atmosphere using a set of elevation angles corresponding to discrete air masses [*Han and Westwater*, 2000]. The consistently cloudy conditions during EPIC did not allow for many tipping curve calibrations; for a 2.5-day period (16 October 1200 UTC until 19 October 0000 UTC), the 31 GHz system gain changed significantly and a tipping curve could not be done. For this time period, only the mailbox radiometer data is used.

2.2. Statistical Variance Analysis

[14] Small-scale system gain variability contributes to variability in T_b approximately as

$$|\delta T_b| = CF * \left(\overline{V_m} - \overline{V_r}\right) * |\delta G| \qquad (2)$$

where δG is the standard deviation in the system gain G for each frequency and $\overline{V_m}$ and $\overline{V_r}$ are mean values. The data were evaluated at a 1-min time resolution. The T_b variability over a 9-day time period was 0.33 K for the 20 GHz channel, comparable to land-based systems. The 31 GHz gain was steadiest from 13 October until 16l October, corresponding to a δT_b of 1.1 K over 1 min. After 19 October, this increased to a δT_b of 2.6 K. The 90 GHz gain not only fluctuated but had a decreasing trend with time, and its data were eliminated from use in this paper.

[15] The 31 GHz T_b variability is significantly higher than the 0.3–0.5 K calibration error typical of land-based systems [*Mattioli et al.*, 2005; *Westwater et al.*, 2003, 2001]. The large degree of 31 GHz instrument noise primarily reflects variations in the reference blackbody voltage V_r. It should be noted that the same instrument possessed a much steadier calibration, with a δT_b of 0.3 K or less, when producing the data analyzed by *Albrecht et al.* [1990]. The increased system gain variability experienced during EPIC may reflect the more difficult electronic environment of a ship, or may simply be instrument age. In either case, the high amount of small-scale variability should be considered when further applying the data.

[16] The 20 GHz instrument uncertainty of 0.33 K translates into a LWP uncertainty of ∼6 g m^{-2}, while 31 GHz T_b uncertainties of 1.1 and 2.6 K propagate into LWP uncertainties of ∼40 and 90 g m^{-2}, respectively, for data at 1-min sampling (see Appendix B). We further averaged the data into 10-min time intervals, decreasing T_b and LWP uncertainties by a factor of 10$^{-0.5}$ (i.e., the 1-min system gain time series fluctuates as random, uncorrelated noise). At this timescale, the 20 GHz T_b is accurate to 0.1 K and the 31 GHz T_b is accurate to 0.35 K or 0.9 K depending on the time period. The total LWP uncertainty, at 10-min time resolution, caused by variability in both Hughes MWR frequencies, is therefore ∼15 g m^{-2} from 13 October until 16 October and ∼30 g m^{-2} after 19 October.

2.3. Dual-Instrument Comparison

[17] The calibrated Hughes MWR measurements were compared to those from the mailbox MWR. The T_b from the vapor-sensitive channels are shown in Figure 1a; most data follow a linear relationship, as theoretically expected. As a quality control, T_b deviating by more than 1 K from the best fit line were removed from the data set. A subset in time of the T_b from the two liquid-sensitive channels is shown in Figure 1b. These compare poorly. The mailbox 31.4 GHz brightness temperatures are ∼2 K higher than the Hughes 31.65 GHz brightness temperatures. For a later time period (not shown), the opposite relationship occurs at high T_b. The cause is attributed to mailbox radiometer calibration shifts occurring throughout the experiment, with none of them apparently correct, possibly as a result of the persistently cloudy conditions.

3. Evaluation of Gaseous Absorption Models

[18] Gaseous absorption occurs from water vapor, oxygen, and nitrogen. Three gaseous absorption models, each modeling all three gases, were evaluated. The *Liebe and Layton* [1987] model (hereinafter referred to as Lieb87) is implemented in the operational statistical retrievals of the
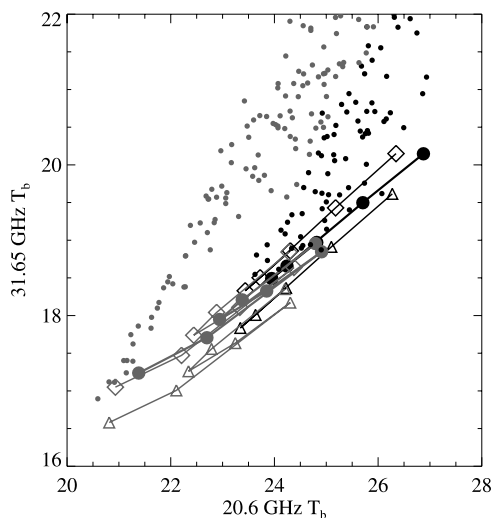
Figure 2. Measured brightness temperatures on 14 and 15 October (solid and shaded circles, Hughes MWR), calculated clear-sky T_b using the Lieb87, R98, and Lilj05 gaseous absorption models (triangles, diamonds, and solid circles), with black and grey indicating coincidence with sondes on 14 and 15 October, respectively.

NOAA ETL ship-based field experiments; either it or a similar precursor were used for the retrieved LWPs shown by *Albrecht et al.* [1990], *Fairall et al.* [1990], and *Bretherton et al.* [2004]. It was used operationally by the ARM program up to April 2002. The second model, that of *Rosenkranz* [1998] (hereinafter referred to as R98) is recommended for very dry Arctic atmospheres by [*Westwater et al.* 2001], is used by *Löhnert et al.* [2004], and has also been evaluated by *Marchand et al.* [2003], *Westwater et al.* [2003], and *Mattioli et al.* [2005]. It became the ARM standard after April 2002. The third model is the most recent, that of *Liljegren et al.* [2005] (hereinafter referred to as Lilj05). 31 GHz brightness temperatures calculated from high-quality Vaisala RS90 sondes with the Lilj05 model compared most favorably to clear-sky MWR measurements of five models evaluated at the Oklahoma Atmospheric Radiation Measurement (ARM) site [*Mattioli et al.*, 2005], primarily because of an improved representation of the water vapor continuum at 31 GHz.

[19] No unambiguous clear-sky EPIC soundings (as determined from a ceilometer, cloud radar, and MWR T_b) were identified for days when the Hughes radiometer was relatively stable. However, we can still examine whether sonde-calculated values of T_b (which don't include liquid) are lower than the measured T_b, which do include a response to liquid. This is shown in Figure 2 for 14 and 15 October. The 11 sondes sampled a range of sonde-calculated water vapor paths from 1.4 to 2.0 cm.

[20] As shown in Figure 2, differences in clear-sky T_b calculated by the three models can reach ∼0.5 K (R98-Lieb87), corresponding to a LWP difference of ∼15 g m^{-2}. The R98 appears to slightly overestimate, but does the Lieb87 model underestimate clear-sky T_b? In a comparison of truly clear-sky conditions, *Marchand et al.* [2003] found that the Lieb87 model underestimates and the R98 model overestimates the true clear-sky T_b for this range of water

vapor paths. *Mattioli et al.* [2005] found better agreement using the R98 model rather than the Lieb87 model to the measured clear-sky T_b at the Oklahoma ARM site, particularly for the water vapor channel, and a slight overestimate in the 31 GHz values at higher water vapor paths with the R98 model.

[21] Figure 2 demonstrates a best fit to the data by the Lilj05 model; its choice finds further strong support from the studies of *Mattioli et al.* [2005] and *Marchand et al.* [2003]. *Mattioli et al.* [2005] compared radiosonde-calculated 31 GHz T_b (from applying the Lilj05 model to ∼70 Vaisala RS90 sondes) to three different MWRs, calibrated in two different ways, and found absolute biases of 0.2 K and often less than 0.1 K, with root-mean-square deviations of ∼0.3 K. In addition, the Lilj05 model was the only model examined for which the residuals exhibited no dependence on the 31 GHz T_b. An uncertainty of 0.2 K, conservatively assigned, corresponds to a LWP uncertainty of ∼6 g m^{-2} from the gaseous absorption model alone. The Lilj05 model is similar to R98 at low water vapor paths, but generates a shallower slope than the two other models. The T_b produced by the Lilj05 model imply that in dry atmospheres it will produce retrieved LWPs similar to that of the R98 model and lower than those from the Lieb87, while in moister environments (water vapor path approximately ≥1.7 cm) the Lilj05 model will produce retrieved LWPs lower than those from the Lieb87 model, and higher than those from the R98 model.

4. Liquid Water Path Retrieval

[22] Different techniques exist for retrieving liquid water paths. Statistical retrievals are common; these build on long-term statistics at one site and substitute the climatological vertical cloud distribution for the instantaneous cloud distribution. This approach works less well for short-term field experiments held in remote locations, for which long-term statistics do not exist. The approach that achieves the most accurate LWP values possible with a two-channel radiometer is a physical-iterative method [*Han and Westwater*, 1995; *Liljegren et al.*, 2001], which implements the cloud temperature as an explicit input into the microwave radiative transfer. This takes into consideration the strong temperature dependence of the liquid dielectric constant: at microwave frequencies, colder clouds possess the counter-intuitive quality of being more opaque and radiating more brightly than warmer clouds of the same liquid water path.

[23] Within the physical-iterative retrieval, sounding temperature and humidity data and cloud boundaries serve as physical inputs into a forward model, and an iterative search locates the LWP most physically consistent with the measured MWR T_b. A physical-iterative approach is particularly useful for a stratocumulus regime, where cloud boundaries are easily determined with a cloud base ceilometer, and cloud radar or sonde data. The reliance on interpolated sonde humidities preserves the vertical structure. This approach, which no longer uses the 22 GHz T_b to estimate short-term moisture variability, has the most utility for regions with limited variability in the total water vapor content such as marine stratocumulus.

[24] The LWP retrieval also takes full advantage of more recently manufactured sondes. The EPIC Vaisala RS80
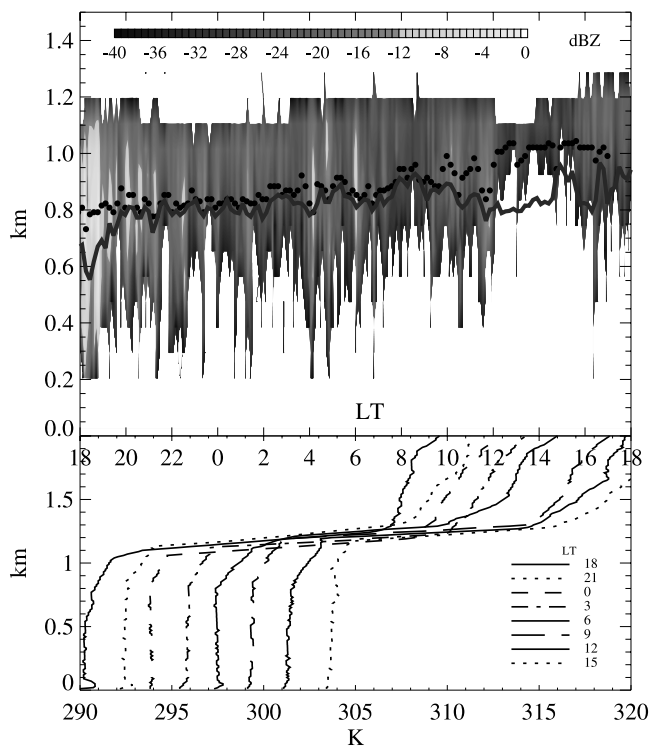
Figure 3. (a) The 15 October cloud radar reflectivities, ceilometer cloud base heights (solid circles), and the lifting condensation level calculated from shipboard flux measurements displaced upward by 150 m (grey line). The radar reflectivities represent the "precipitation mode" of the cloud radar. (b) The 15 October potential temperature soundings, each sounding subsequent to the 1800 LT sounding is displaced by 2 degrees from the previous sounding. All times are local times.

sondes were manufactured well after Vaisala implemented a corrective sealed sensor cap into its packaging [*Wang et al.*, 2002]. (Initial efforts to evaluate gaseous absorption models through comparisons to soundings documented a dry bias in the humidity data of the commonly used Vaisala RS80 sondes [*Westwater et al.*, 2003; *Turner et al.*, 2003].) Recent comparisons find good agreement between the new RS80 sondes and the more accurate chilled-mirror dew point hygrometers [*Miloshevich et al.*, 2004; *Wang et al.*, 2003], with a dry bias only remaining in the upper troposphere, where the contribution to the total water vapor path is small.

[25] The iteration toward a final LWP minimized a cost function involving both the 22 and 31 GHz brightness temperatures:

$$F = \left| T_{b,\text{calc}}^{22}(L) - T_{b,\text{meas}}^{22}(L) \right| + \left| T_{b,\text{calc}}^{31}(L) - T_{b,\text{meas}}^{31}(L) \right| \quad (3)$$

The iteration is continued until $T_{b,\text{calc}}^{31}$ is within 0.1 K of $T_{b,\text{meas}}^{31}$ and not exceeding it, with the LWP responsible for the minimum in the cost function chosen thereafter. In practice, the minimum in the cost function for a given gaseous absorption model is primarily determined by the 31 GHz contribution.

[26] The liquid dielectric models were applied to data from 15 October. Skies were almost consistently overcast on this day with little drizzle (implying a robust ceilometer-based cloud base determination). The temperature and humidity profiles documented by 8 times daily sondes were interpolated to 10-min intervals. The inversion strength varied between 11 and 15 K. The cloud radar reflectivities, ceilometer cloud bases, and potential temperature profiles are shown in Figure 3. The cloud top was established by a radar reflectivity threshold of −35 dBZ, placing the cloud top near the minimum temperature of the temperature inversion. The ceilometer cloud base lies above the lower cloud boundary defined by the cloud radar. This is often observed in stratus clouds. The cloud radar is more responsive to large drop sizes than the ceilometer, and the different cloud boundaries indicates sedimentation and evaporation of some larger drops is occurring below the cloud base.

[27] The lifting condensation level calculated from the ship flux measurements is also shown, displaced upward by 150 m to account for surface layer effects [*Caldwell et al.*, 2005]. During much of the day, the displaced lifting condensation level closely matches the ceilometer cloud base, signifying a relatively well-mixed boundary layer. Decoupling of the cloud from the near surface is most apparent during the time of heaviest drizzle and around solar noon.

4.1. Liquid Dielectric Models

[28] The two liquid dielectric models examined are the *Grant et al.* [1957] model and the *Liebe et al.* [1991] model further modified according to *Liebe et al.* [1993] (hereinafter referred to as the G57 and L91 models). The G57 model has been the standard for ETL ship-based field experiments, was utilized by *Albrecht et al.* [1990], *Fairall et al.* [1990], and *Bretherton et al.* [2004] and was the ARM standard until April 2002. After that the ARM program migrated to the L91 model, based upon the conclusion (drawn from comparisons to aircraft data) that L91 performs better at temperatures below 0°C than the G57 model [*Westwater et al.*, 2001]. The *Liebe et al.* [1991] model was carefully measured in the laboratory and is thought to be accurate at temperatures above 0°C. Other validation is difficult, and we will assume the L91 model is perfectly known.

[29] The impact of the two liquid absorption models were first evaluated in combination with the Lilj05 gaseous absorption model. The L91 model produced LWPs that were 5.6 g m^{-2} lower per 100 g m^{-2} of LWP than the G57 model, with a standard deviation of 0.3 g m^{-2}. The difference reflects a higher liquid mass absorption coefficient for the L91 model, exceeding the G57 coefficients by ∼5% at typical stratus cloud temperatures. Higher coefficients, for the same optical depth, generate lower retrieved LWPs.

[30] When combined with the three gaseous absorption models, a clear trend with development age is evident, with the more recent model combinations producing lower LWPs. A combination of six (gas, liquid) absorption models are possible. Five of these are depicted in Figure 4, reflecting the range of possibilities; a grouping by age of development and likelihood of coincident application would be the (Lieb87, G57) combination used by *Albrecht et al.* [1990], *Fairall et al.* [1990], and *Bretherton et al.* [2004],
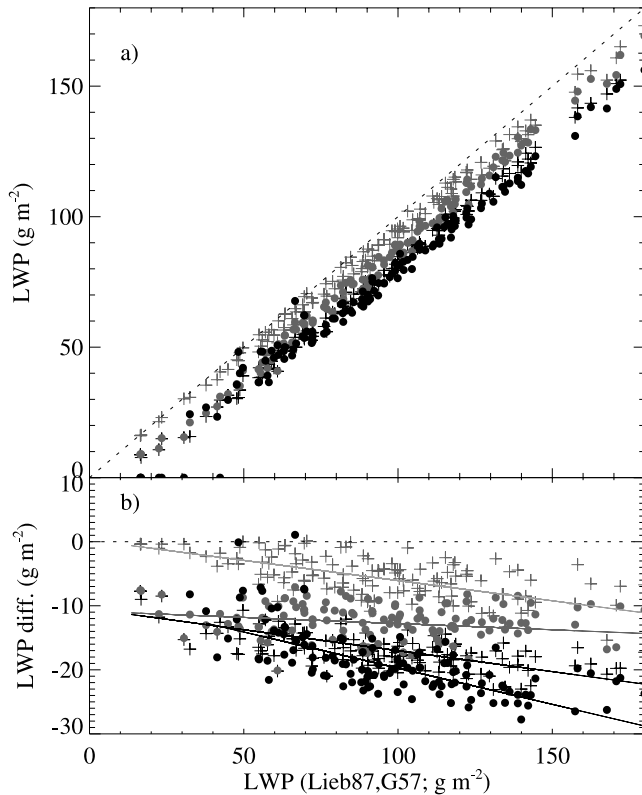
Figure 4. (a) Liquid water paths retrieved for 15 October from Hughes MWR data using the (Lieb87, L91), (R98, L91), (R98, G57), and (Lilj05, L91) models (grey and black pluses, grey and black circles, respectively) versus LWPs retrieved using (Lieb87, G57) model. (b) Similar to Figure 4a but showing the difference between the LWPs retrieved with each model and the (Lieb87, G57) model.

the (R98, L91) combination, which was the ARM standard retrieval from April 2002, until recently, and the most recent model combination (Lilj05, L91). The (Lieb87, L91) and (R98, G57) model combinations are included for the purpose of illustration. The (Lieb87, G57) model values form the x axis of Figure 4, with the other four model combinations forming the y axis in Figure 4a, while Figure 4b shows the LWPs as a difference between the four models and the (Lieb87, G57) model and includes best fit lines.

[31] It is clear that the (Lieb87, G57) model combination produces the highest LWPs. The choice of gaseous absorption model has a greater impact on the retrieved LWPs than the choice of the liquid dielectric model. The R98 gaseous model produces LWPs that are reduced by $\sim$10 g m^{-2} from those produced by the L87 model, and the Lilj05 gaseous absorption model reduces the retrieved LWPs further, by an additional 4 g m^{-2} per 100 g m^{-2}. In combination, the (Lilj05, L91) models produce retrieved LWPs of approximately 80 and 170 g m^{-2} where the (Lieb87, G57) models produce retrieved LWPs of 100 and 200 g m^{-2}, a reduction of 20% and 15%, respectively.

4.2. Comparison to Adiabatic Values

[32] LWPs retrieved with the (Lieb87, G57), (Lieb87, L91), (R98, L91) and (Lilj05, L91) model combinations are compared against adiabatically calculated LWP values in

Figure 5. The adiabatic calculation is similar to that of *Albrecht et al.* [1990]:

$$LWP = 0.5 \frac{\rho}{\rho_l} \Gamma_l (z_t - z_b)^2 \qquad (4)$$

$$\Gamma_l = -\frac{dw_s}{dz} \qquad (5)$$

where w_s is the saturation mixing ratio, ρ is the air density at cloud center, ρ_l is the density of water, and z_t and z_b are cloud top height and base. Γ_l depends on the moist adiabatic lapse rate, which is calculated according to equation (3.15) of *Houghton* [1986] and the cloud center pressure and temperature. This calculation of Γ_l was found to closely match another independent calculation relying on equations from *Pruppacher and Klett* [1978]. The calculation does not consider the variation in Γ_l with height, but cloud center values deviated from those at cloud top and cloud base by <3%.

[33] The cloud base was determined through a ceilometer, and the cloud top established through a radar reflectivity threshold of −35 dBZ. This placed the cloud top at or close to the minimum of the temperature inversion. The cloud base has a manufacturer-specified uncertainty of 30 m, and the cloud top uncertainty is primarily determined by the vertical resolution of the cloud radar, or 90 m. Difficulty in
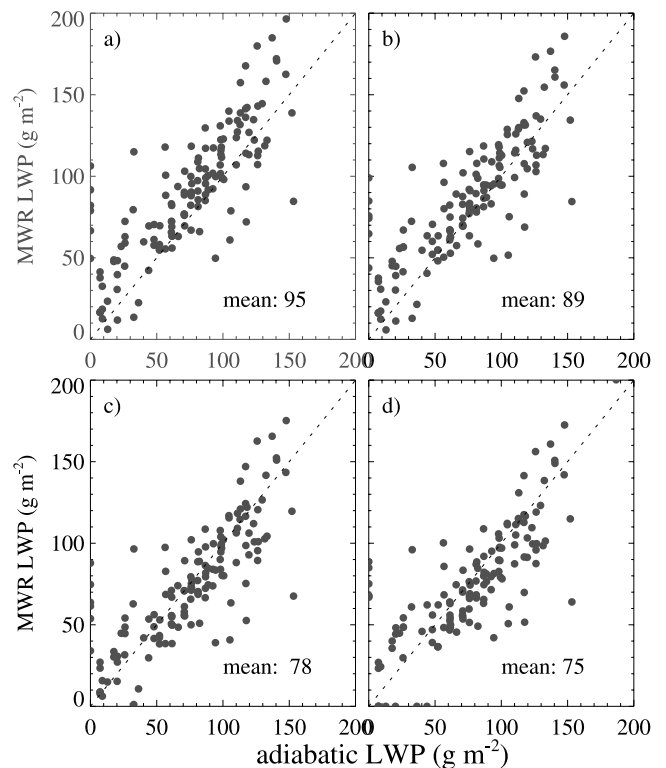

Figure 5. (a) Liquid water paths retrieved using the (Lieb87, G57) models, (b) (Lieb87, L91) models, (c) (R98, L91) models, and (d) (Lilj05, L91) models versus adiabatically calculated LWPs. The mean retrieved LWP for each model combination is indicated in Figures 5a–5d. Data are from the Hughes MWR on 15 October.
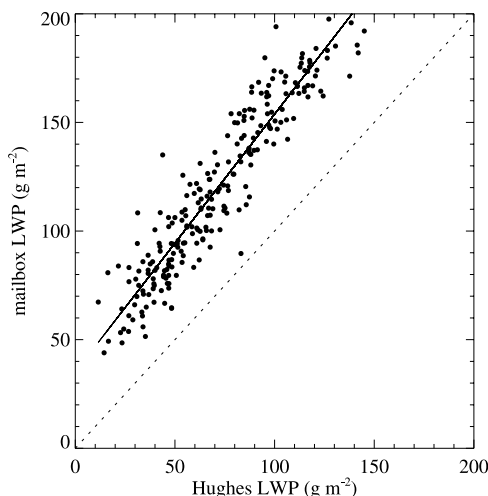
Figure 6. Liquid water paths retrieved from the mailbox radiometer T_b measurements versus those retrieved from the Hughes MWR T_b for 15–16 October 1200 UTC and 19 October. Retrievals rely on the Lilj05 and L91 absorption models. LWPs are retrieved from the same measurements shown in Figure 1b.

precisely placing the cloud top is arguably the largest source of uncertainty in the adiabatic LWP determination. An assumed uncertainty in the cloud thickness of 50 m corresponds to an uncertainty in the adiabatic LWP of $\sim$25 g m^{-2}.

[34] The comparisons are shown in Figure 5 with mean nonzero retrieved LWP values shown in Figure 5d. The mean nonzero adiabatic LWP is 78 g m^{-2}. Figures 5a and 5b correspond to the Lieb87 gas model; clearly the Lieb87 gas model produces LWPs that tend to exceed the adiabatic maximum (also evident in a best fit line), regardless of the liquid dielectric model. Figure 5c, the (R98, L91) model combination, shows a better correspondence to the adiabatic values. The retrieved LWPs are further reduced using the most recent (Lilj05, L91) model combination, but less so. The total range in retrieved LWPs for the four different model combinations is 20 g m^{-2}, or more than 20% of the total.

5. The 16–22 October Time Series

[35] A best estimate LWP time series was constructed using the Lilj05 gaseous absorption model and the L91 liquid dielectric model. The time series encompasses 16–22 October, during which time the R/V *Ronald Brown* was stationed at 20°S, 85°W, $\sim$700 km off of the Peruvian/Chilean border. The sky was usually overcast, with a regular predawn maximum and afternoon minimum in drizzle and cloud thickness [*Bretherton et al.*, 2004].

[36] The time series consists of the Hughes LWP values when they are available. As a quality control, 31 GHz measurements that were physically implausible as a function of the coincident 20 or 23 GHz measurements were eliminated (these were few). From 16 October 1200 UTC to 19 October 0000 UTC, the mailbox-derived LWP values were corrected for their mean overestimate of $\sim$40 g m^{-2} using a regression developed from near-in-time coincident

Hughes and mailbox LWP values, shown in Figure 6 (from the same data shown in Figure 1b). The regression is [mailbox LWP] = 35.06 + 1.19 [Hughes LWP] with 1-sigma uncertainties of [2.1, 0.0263]. The uncertainty introduced through the regression is therefore $\sim$5 g m^{-2}; when combined with that from the Hughes instrument gain variability, the total uncertainty in the 10-min LWP values during 16–19 October is estimated at 35 g m^{-2}. Figure 7 shows the surface-derived LWPs from 16 October until 22 October.

6. Implications for Cloud Processes

6.1. Comparison to Adiabatic Values

[37] How well do the retrieved LWPs compare to the theoretical adiabatic maximum? Figure 8 shows all retrieved values, including during drizzle, as a function of the adiabatic value (see Appendix A for a discussion on the impact of drizzle on the LWP retrieval). The retrieved values, despite being decreased from earlier estimates using older microwave absorption models, are still remarkably close to the adiabatic limit for LWPs up to 150 g m^{-2}. Thereafter mean retrieved LWPs decrease to $\sim$85% by a LWP of 250 g m^{-2}; conclusions cannot be drawn for higher LWPs. The physical implication is that there is little impact upon the liquid water contents from entrainment or drizzle until LWPs exceed 200 g m^{-2}. This conclusion does rest on the determination of cloud thickness, to which the adiabatic calculation is sensitive. Although the conclusion is similar to that of *Albrecht et al.* [1990], it should be noted that application of the recent microwave models would have resulted in lowered retrieved LWPs, by $\sim$20%, for the results shown by *Albrecht et al.* [1990].

6.2. Relationship to Drizzle

[38] At what LWP does drizzle begin to occur in stratus clouds? Microwave LWP retrievals do not consider drop size; this assumption is adequate in all but the heaviest of stratus precipitation events because drizzle water contents are usually low (Appendix A). Drizzle is inferred from the "precipitation mode" cloud radar reflectivities. As shown in
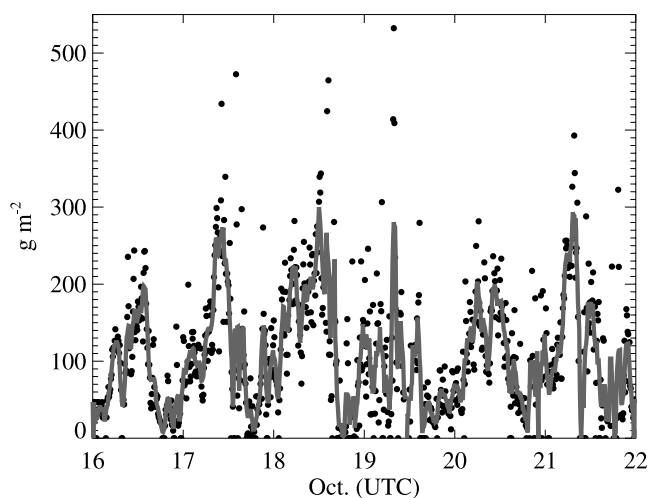

Figure 7. Time series of retrieved LWPs for 16–22 October. The grey line is a smoothed interpolation.
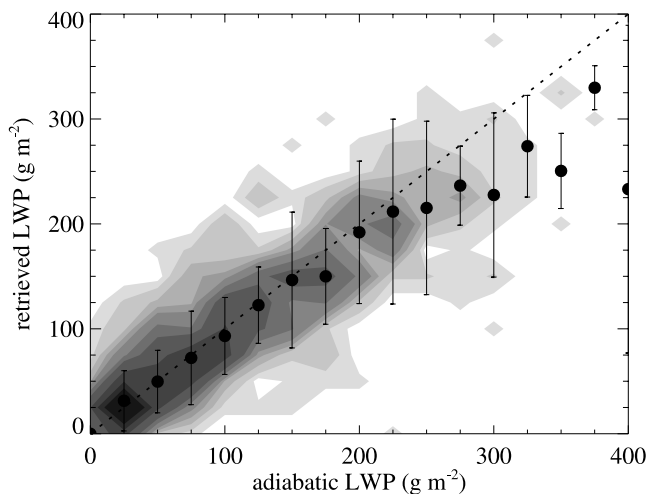
Figure 8. Contoured frequencies of retrieved versus adiabatic LWPs, 16–22 October, 10-min resolution. Contours at 0.1, 0.25, 0.5, 0.75, 1.0, 1.5, 2.0, 3.0, 4.0, 5.0 frequencies, 25 g m^{-2} bins. Solid circles and bars indicate mean retrieved LWPs for each 25 g m^{-2} bin of adiabatic LWP and their standard deviation.

Figure 9a, very light drizzle (dBZ > −17, corresponding to a cloud base drizzle rate of ∼0.01 mm d^{-1} [*Comstock et al.*, 2004]) can occur even in clouds with low liquid water paths (∼10 g m^{-2}), though its likelihood of occurrence increases strongly with LWP (correlation coefficient of 0.75). Heavy drizzle (dBZ > 0, corresponding to a cloud base drizzle rate of ∼2 mm d^{-1} [*Comstock et al.*, 2004]) is unlikely until a LWP of ∼125 g m^{-2} and still occurs <10% of the time at LWPs of ∼200 g m^{-2} (Figure 9b).

[39] Several studies discuss a recycling of drizzle water back into a cloud, either through a reintroduction of the evaporated vapor, or as a physical "relifting" at eddy scales for light drizzle [*Vali et al.*, 1998], and as part of a mesoscale moist updraft subcloud circulation [*Comstock et al.*, 2005]. The high sensitivity of the cloud radar to drizzle is allowing a separate identification of very light drizzle. The recycling of drizzle back into the cloud is aided by the relatively well mixed boundary layer and high cloud bases typifying EPIC (see, e.g., Figure 3 and *Bretherton et al.* [2004]), helping to explain the coexistence of drizzle with LWPs close to the adiabatic maximum. Small drizzle amounts are also more likely to evaporate near cloud base, evident in Figure 3, with the resulting cooling furthering the destabilization and mixing of the boundary layer [*Feingold et al.*, 1996].

6.3. Diurnal Cycle

[40] As evident in Figure 7, a strong diurnal cycle in LWP prevailed during the 6 days. Figure 10 shows the 6-day diurnal cycle composite in the retrieved and adiabatic LWPs as well as in the frequency of occurrence of drizzle. The 6-day averaging further reduces the errors on the retrieved LWPs, to 3 g m^{-2}. Figure 10 again confirms that the clouds are close to adiabatic throughout much of the day, with the largest deviation occurring between 0200 and 0700 LT, when drizzle is also most prevalent. Light drizzle occurs at almost all times of day, with a minimum at local noon,

when the LWPs also reach their minimum, and the boundary layer is least well mixed [*Comstock et al.*, 2005]. Heavy drizzle possesses a more pronounced diurnal cycle than light drizzle and is most prevalent between 0100 and 0800 LT. Again, the light drizzle does not appear to encourage deviations of the cloud from adiabatic values. Variations in adiabatic LWPs occurring at the 10-min timescale are well captured by the retrieved LWPs.

7. Summary

[41] We reexamine liquid water paths derived within marine stratus regions using the most recent microwave absorption models. The *Liljegren et al.* [2005] gaseous absorption model has previously been shown to produce the most accurate 31 GHz T_b of five examined models [*Mattioli et al.*, 2005], with biases and root-mean-square deviations of less than 0.2 K and 0.35 K from radiosonde-calculated T_b for three different MWRs, calibrated in two different ways. This reflects an improved model depiction of the water vapor continuum at 31 GHz. The Lilj05 model reduces LWP estimates by 10–20 g m^{-2} from pre-1995 values, with the largest reductions occurring at lower water vapor paths (e.g., Figure 2). The Lilj05 model is estimated to produce LWPs accurate to ∼6 g m^{-2}, based on the work by *Mattioli et al.* [2005].

[42] The *Liebe et al.* [1991] liquid model has been measured in the laboratory and is thought to be accurate for temperatures above 0°C [*Westwater et al.*, 2005]; it reduces the LWP estimate from that produced by the G57 model by almost 6 g m^{-2} per 100 g m^{-2}, at EPIC stratocumulus cloud temperatures. In tandem, the (Lilj05, L91) model combination decrease the retrieved stratus LWPs from earlier estimates by ∼10–25 g m^{-2}, dependent on LWP and the water vapor path. The impact upon retrieved LWPs is larger from improvements in the gaseous absorption models rather than the liquid dielectric models;
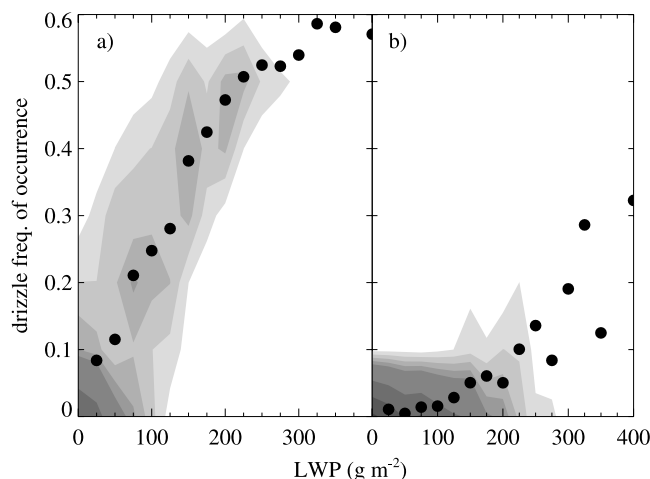

Figure 9. (a) Contoured frequencies of the occurrence of drizzle, measured as the fraction of radar reflectivities exceeding −17 dBZ versus retrieved LWP. Contours at 0.05, 0.1, 0.15, 0.2, 0.25, 0.5, 0.75, 1.0, 1.5, 2.0 frequencies, 25 g m^{-2} bin. Solid circles indicate the mean drizzle frequency of occurrence as a function of LWP. (b) Same as Figure 9a but for radar reflectivities >0 dBZ.
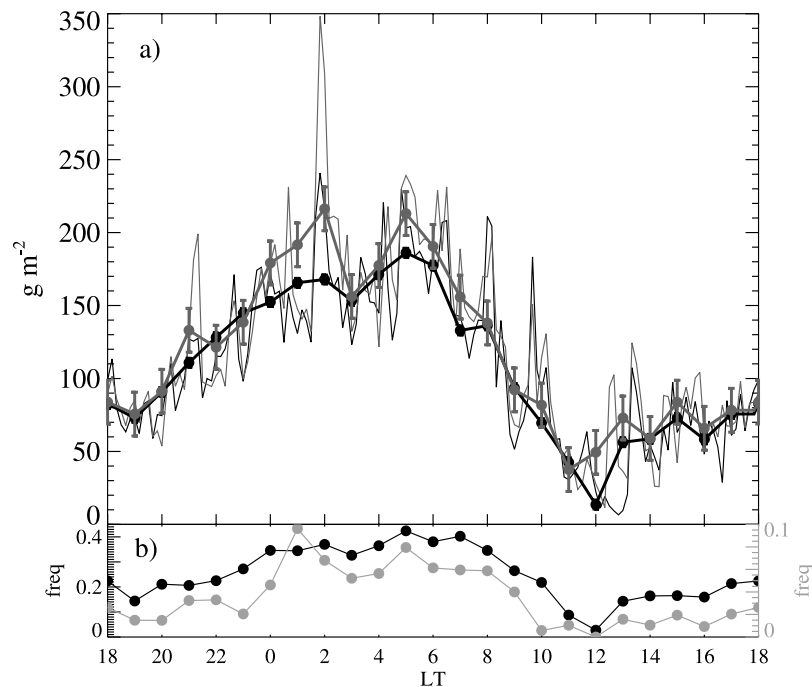
Figure 10. (a) Retrieved LWPs (black line) and adiabatic values (grey line), at 10-min resolution (thin lines) and as hourly mean values (thick lines with circles and error bars of ~25 g m^{-2} for the adiabatic values, respectively), averaged over the buoy time period, as a function of local time. (b) Diurnal cycle at buoy in the frequency of occurrence of radar reflectivities exceeding −17 and 0 dBZ (black and grey circles, corresponding with left- and right-hand y axes) as a function of local time.

this contrasts to the Arctic, where changes in the liquid dielectric models appear to have equal or greater impact [*Westwater et al.*, 2001].

[43] There are several implications of the microwave model improvements for stratocumulus clouds. First, the updated models allow for a new evaluation of the adiabaticity of marine stratocumulus clouds. For the 6-day time period under examination, the most recent models retrieve cloud liquid water paths close to their adiabatic maximum up to LWPs of 150 g m^{-2}, diminishing to 85% of adiabatic at a LWP of 250 g m^{-2}. The high degree of adiabaticity is somewhat unique to EPIC. Clouds of similar LWPs appear to be adiabatic in the study by *Albrecht et al.* [1990], but an application of the recent models would have generated (Californian stratocumulus) LWPs ~20% lower, or 80% of the adiabatic maximum. Recent aircraft measurements taken within the Californian stratocumulus regime also find LWPs approximately two thirds of adiabatic (B. Stevens et al., On the structure of the lower troposphere: July 2001 near 120W and 30N, submitted to *Journal of Climate*, 2005). Stratocumulus LWPs in the northern Atlantic are also often observed to be subadiabatic [*Wood*, 2005].

[44] Second, incorporation of the new microwave models allows for an improved evaluation of the occurrence of drizzle as a function of LWP. Light drizzle (radar reflectivities >−17 dBZ, equivalent to a cloud base drizzle rate of ~0.01 mm d^{-1} [*Comstock et al.*, 2004]) is often present even in low liquid water clouds, while heavy drizzle (radar reflectivities >0 dBZ, equivalent to a cloud base drizzle rate of 2 mm d^{-1}) is much less common, approaching a frequency of occurrence of 10% for LWPs of

~200 g m^{-2}. An evaluation of the diurnal cycle further supports the view that only heavy drizzle contributes to cloud deviations away from adiabatic values, mostly in the hours between midnight and 0400 LT.

[45] It is interesting that the southeastern Pacific stratus region, during this time period, appears to have LWPs close to the adiabatic maximum, given that this is not universally common, and that the adiabatic LWPs occur along with the presence of drizzle. It could reflect on the adiabatic calculation, particularly the cloud thickness determination. *Zuidema et al.* [2005], however, found close agreement between aircraft and surface-based determinations of cloud boundaries and LWPs, for one Arctic cloud case study. Part of the explanation resides in the ability of the cloud radar to detect light drizzle, both through its high sensitivity, and its sampling of large volumes. Aircraft measurements cannot sample large volumes, and may tend to underestimate the frequency of light drizzle.

[46] One physical explanation (for the coexistence of adiabatic LWPs and drizzle) may reside in the high cloud bases typical of the EPIC stratus experiment (see Figure 3, as well as *Bretherton et al.* [2004]), which, given the relatively well mixed boundary layer, fosters the recirculation of drizzle (as either liquid or vapor) back into the cloud on both eddy scales [*Vali et al.*, 1998] and mesoscales [*Comstock et al.*, 2005], rather than allowing the drizzle to reach the surface. Modeling work has also highlighted the distinct impacts on boundary layer dynamics of small drizzle amounts, which tend to evaporate close to cloud base and thereby destabilize the boundary layer and encourage mixing, and larger drizzle amounts capable of reaching

near the surface and stabilizing the boundary layer [*Feingold et al.*, 1996]. With this is mind, the threshold distinguishing drizzle from cloud will have bearing on what conclusions are drawn regarding drizzle impacts, as smaller drops are more likely to evaporate near cloud base. Thresholds can vary from 20 μm [*Wood*, 2005; *Comstock et al.*, 2004] and upward to at least 100 μm.

[47] Third, the decrease in the retrieved LWPs with the newer microwave models has implications for microphysical retrievals based on the LWPs. For example, LWPs retrieved from MWR data during the Azores Stratocumulus Transition Experiment utilized the Lieb87 and G57 models. The approximate 20% mean overestimate in LWP will translate to an overestimate in the retrieved effective drop sizes of 8% using the technique of *Frisch et al.* [1995] and of 15% in the cloud optical depths as derived by *Zuidema and Evans* [1998]. Microwave satellite LWP retrievals such as presented by *Wentz* [1997] rely on models similar to the *Liebe and Layton* [1987] gaseous absorption model and the *Grant et al.* [1957] liquid dielectric model, and thus satellite microwave LWP retrievals may also be overestimated as a result.

[48] We note that many American ship experiments, present and future, rely on the two microwave radiometers examined in this paper. The contribution of instrument noise to the EPIC 31 GHz T_b is $3-6$ times higher than is typical of land-based systems and warns that care should be taken when applying the data in further retrievals. It is not known at this time if the EPIC experience is representative for other field campaign ship-based MWR data. The ETL radiometer was used for the results of *Albrecht et al.* [1990]; the radiometer possessed a more accurate calibration (<0.3K) then than prevailed during EPIC.

Appendix A

[49] An assumption embedded in the LWP retrieval is that the liquid absorption is solely dependent upon the LWP and independent of drop size, called the Rayleigh assumption. The absorption calculated using the more exact Mie theory deviates ~5% from that calculated with the Rayleigh assumption at a radius of 100 μm and 20% at a radius of 200 μm [*Petty*, 1990]. Nevertheless, even in heavily drizzling conditions, the amount of LWP contained in drizzle drops exceeding 200 μm is so small, that their increased contribution to the total mass extinction coefficient and thereby the retrieved LWP can be effectively ignored.

[50] This is brought out by a crude but effective calculation, utilizing the EPIC drizzling drop size distributions presented by *Comstock et al.* [2004]. They conclude that for 5% of the drizzling situations during EPIC, cloud base rain rates exceed 0.37 mm h^{-1}, or almost 9 mm d^{-1} (evaporation will decrease subcloud base rain rates). They also find a mean drizzle drop size at cloud base of 40 ± 20 μm for all EPIC drizzle conditions, using a drizzle threshold drop size of 20 μm. If we assume a drizzle rate of 0.5 mm h^{-1} (12 mm d^{-1}) and a mean drizzle drop size of 50 μm in their equation (9), we determine a drizzle drop concentration of 100 L^{-1}. The corresponding cloud base drizzle water content is 0.125 g m^{-3}, of which 0.015 g m^{-3} is contributed by drops with radii >200 μm. If we assume mean drizzle amounts between the surface and cloud base equal to 0.25 of the cloud base amount (a large underestimate of the evaporative impact), and a cloud base at 1000 m (see, e.g., Figure 3), we arrive at a total drizzle LWP of 31 g m^{-2}, with drops of radii >200 μm contributing ~3.75 g m^{-2}. The drops >200 μm will enhance the 30 GHz T_b to the same extent as 9.5 g m^{-2} of cloud water, using a Mie extinction efficiency of 2.5 that of the Rayleigh value. The overestimate of LWP by 6 g m^{-2} is within the instrumental uncertainty, despite the almost unrealistic heavy drizzle scenario, and justifies the application of the Rayleigh assumption.

Appendix B

[51] The total LWP uncertainty is calculated from $\delta LWP = |l_{20}\delta\tau_{20}| + |l_{31}\delta\tau_{31}|$, where l_{20}, l_{31} are formed from retrieval coefficients and τ_{20}, τ_{31} are the precipitable water optical depths at each frequency. The $\delta\tau = \frac{\delta\tau}{\delta T_b}\delta T_b = \delta T_b/T_{mr} - T_b$, from $\tau = \ln(T_{mr} - T_c/T_{mr} - T_b)$ and using mean values for T_{mr} and T_b. T_{mr} is the mean atmospheric radiating temperature, and T_c is the cosmic background radiating temperature of 2.73 K. *Liljegren et al.* [2001] provide more detail on the derivation of l_{20} and l_{31}, which are equivalent to their equation (4b) coefficients.

References

Albrecht, B. A., C. Fairall, D. Thomson, A. White, and J. Snider (1990), Surface-based remote sensing of the observed and the adiabatic liquid water content, *Geophys. Res. Lett.*, *17*, 89–92.

Bretherton, C. S., T. Uttal, C. Fairall, S. E. Yuter, R. A. Weller, D. Baumgardner, K. Comstock, R. Wood, and G. B. Raga (2004), The EPIC 2001 stratocumulus study, *Bull. Am. Meteorol. Soc.*, *85*, 967–977.

Cahalan, R. F., W. Ridgeway, W. J. Wiscombe, T. L. Bell, and J. B. Snider (1994), The albedo of fractal stratocumulus clouds, *J. Atmos. Sci.*, *51*, 2434–2455.

Caldwell, P., C. S. Bretherton, and R. Wood (2005), Mixed-layer budget analysis of the diurnal cycle of entrainment in SE Pacific stratocumulus, *J. Atmos. Sci.*, *62*, 3775–3791.

Comstock, K. K., R. Wood, S. E. Yuter, and C. S. Bretherton (2004), Reflectivity and rain rate in and below drizzling stratocumulus, *Q. J. R. Meteorol. Soc.*, *130*, 2891–2918.

Comstock, K. K., C. S. Bretherton, and S. E. Yuter (2005), Mesoscale variability and drizzle in southeastern Pacific stratocumulus, *J. Atmos. Sci.*, *62*, 3792–3807.

Decker, M. T., and J. A. Schroeder (1991), Calibration of ground-based microwave radiometers for atmospheric remote sensing, *NOAA Tech. Memo. ERL WPL-197*, 84 pp.

Dong, X., T. P. Ackerman, and E. E. Clothiaux (1998), Parameterizations of the microphysical and shortwave radiative properties of boundary layer stratus from ground-based measurements, *J. Geophys. Res.*, *103*, 31,681–31,693.

Fairall, C. W., J. E. Hare, and J. B. Snider (1990), An eight-month sample of marine stratocumulus cloud fraction, albedo, and integrated liquid water, *J. Clim.*, *3*, 847–864.

Feingold, G., B. Stevens, W. R. Cotton, and A. S. Frisch (1996), The relationship between drop in-cloud residence time and drizzle production in numerically simulated stratocumulus clouds, *J. Atmos. Sci.*, *53*, 1108–1122.

Feingold, G., W. L. Eberhard, D. E. Veron, and M. Previdi (2003), First measurements of the Twomey indirect effect using ground-based remote sensors, *Geophys. Res. Lett.*, *30*(6), 1287, doi:10.1029/2002GL016633.

Frisch, A. S., C. W. Fairall, and J. B. Snider (1995), Measurement of stratus cloud and drizzle parameters in ASTEX with a K_α-band Doppler radar and a microwave radiometer, *J. Atmos. Sci.*, *52*, 2788–2799.

Frisch, A. S., G. Feingold, C. W. Fairall, T. Uttal, and J. B. Snider (1998), On cloud radar and microwave radiometer measurements of stratus cloud liquid water profiles, *J. Geophys. Res.*, *103*, 23,195–23,197.

Grant, E. H., J. Buchanan, and H. F. Cook (1957), Dielectric behavior of water at microwave frequencies, *J. Chem. Phys.*, *26*, 156–161.

Han, Y., and E. R. Westwater (1995), Remote sensing of tropospheric water vapor and cloud liquid water by integrated ground-based sensors, *J. Atmos. Ocean. Technol.*, *12*, 1050–1059.

Han, Y., and E. R. Westwater (2000), Analysis and improvement of tipping calibration for ground-based microwave radiometers, *IEEE Trans. Geosci. Remote Sens.*, *38*, 1260–1277.

Hartmann, D. L., M. E. Ockert-Bell, and M. L. Michelsen (1992), The effect of cloud type on Earth's energy balance: Global analysis, *J. Clim.*, *5*, 1281–1304.

Houghton, J. T. (1986), *The Physics of Atmospheres*, 2nd ed., Cambridge Univ. Press, New York.

Liebe, H., and D. H. Layton (1987), Millimeter wave properties of the atmosphere: Laboratory studies and propagation modeling, *Rep. 87-24*, 74 pp., Natl. Telecommun. and Inf. Admin., Washington, D. C.

Liebe, H. J., G. A. Hufford, and T. Manabe (1991), A model for the complex permittivity of water at frequencies below 1 tHz, *Int. J. Infrared Millimeter Waves*, *12*, 659–675.

Liebe, H. J., G. A. Hufford, and M. G. Cotton (1993), Propagation modeling of moist air and suspended water/ice particles at frequencies below 1000 GHz, in *Atmospheric Propagation Effects through Natural and Man-Made Obscurants for Visible through MM-wave radiation*, *AGARD Conf. Proc.*, *542*, 3.1–3.10.

Liljegren, J. C., E. E. Clothiaux, G. G. Mace, S. Kato, and X. Q. Dong (2001), A new retrieval for cloud liquid water path using a ground-based microwave radiometer and measurements of cloud temperature, *J. Geophys. Res.*, *106*, 14,485–14,500.

Liljegren, J. C., S. A. Boukabara, K. Cady-Pereiria, and S. A. Clough (2005), The effect of the half-width of the 22-GHz water vapor line on retrievals of temperature and water vapor profiles with a twelve-channel microwave radiometer, *IEEE Trans. Geosci. Remote Sens.*, *43*, 1102–1108.

Löhnert, U., G. Feingold, T. Uttal, A. S. Frisch, and M. D. Shupe (2003), Analysis of two independent methods for retrieving liquid water profiles in spring and summer Arctic boundary clouds, *J. Geophys. Res.*, *108*(D7), 4219, doi:10.1029/2002JD002861.

Löhnert, U., S. Crewell, and C. Simmer (2004), An integrated approach toward retrieving physically consistent profiles of temperature, humidity, and cloud liquid water, *J. Appl. Meteorol.*, *43*, 1295–1307.

Marchand, R., T. Ackerman, E. R. Westwater, S. A. Clough, K. Cady-Pereira, and J. C. Liljegren (2003), An assessment of microwave absorption models and retrievals of cloud liquid water using clear-sky data, *J. Geophys. Res.*, *108*(D24), 4773, doi:10.1029/2003JD003843.

Mattioli, V., E. R. Westwater, S. I. Gutman, and V. R. Morris (2005), Forward model studies of water vapor using scanning microwave radiometers, global positioning system, and radiosondes during the Cloudiness Inter-Comparison experiment, *IEEE Trans. Geosci. Remote Sens.*, *43*, 1012–1021.

McFarlane, S. A., and K. F. Evans (2004), Clouds and shortwave fluxes at Nauru. Part II: Shortwave flux closure, *J. Atmos. Sci.*, *61*, 2602–2615.

Miloshevich, L. M., A. Paukkunen, H. Volmel, and S. J. Oltmans (2004), Development and validation of a time-lag correction for Vaisala radiosonde humidity measurements, *J. Atmos. Sci.*, *21*, 1305–1327.

Petty, G. (1990), On the response of the Special Sensor Microwave/Imager to the marine environment: Implications for atmospheric parameter retrievals, Ph.D. thesis, Univ. of Wash., Seattle.

Pruppacher, H. R., and J. D. Klett (1978), *Microphysics of Clouds and Precipitation*, Springer, New York.

Rosenkranz, P. W. (1998), Water vapor microwave continuum absorption: A comparison of measurements and models, *Radio Sci.*, *33*, 919–928.

Turner, D., B. M. Lesht, S. A. Clough, J. C. Liljegren, H. E. Revercomb, and D. C. Tobin (2003), Dry bias and variability in Vaisala RS80-H radiosondes: The ARM experience, *J. Atmos. Ocean. Technol.*, *20*, 117–132.

Vali, G., R. D. Kelly, J. French, S. Haimov, D. Leon, R. E. McIntosh, and A. Pazmany (1998), Finescale structure and microphysics of coastal stratus, *J. Atmos. Sci.*, *55*, 3540–3564.

Wang, J., H. Cole, D. J. Carlson, E. R. Miller, K. Beierle, A. Paukkunen, and T. K. Laine (2002), Corrections of humidity measurement errors from the Vaisala RS80 radiosonde: Application to TOGA-COARE, *J. Atmos. Oceanic Technol.*, *19*, 981–1002.

Wang, J., D. J. Carlson, D. B. Parsons, T. F. Hock, D. Lauritsen, H. L. Cole, K. Beierle, and E. Chamberlain (2003), Performance of operational radiosonde humidity sensors in direct comparison with a chilled mirror dewpoint hygrometer and its climate implication, *Geophys. Res. Lett.*, *30*(16), 1860, doi:10.1029/2003GL016985.

Wentz, F. J. (1997), A well-calibrated ocean algorithm for Special Sensor Microwave/Imager, *J. Geophys. Res.*, *102*, 8703–8718.

Westwater, E. R., Y. Han, M. D. Shupe, and S. Y. Matrosov (2001), Analysis of integrated cloud liquid and precipitable water vapor retrievals from microwave radiometers during the Surface Heat Budget of the Arctic Ocean project, *J. Geophys. Res.*, *106*, 32,019–32,030.

Westwater, E. R., B. B. Stankov, D. Cimini, Y. Han, J. A. Shaw, B. M. Lesht, and C. N. Long (2003), Radiosonde humidity soundings and microwave radiometers during Nauru99, *J. Atmos. Ocean. Technol.*, *20*, 953–971.

Westwater, E. R., S. Crewell, and C. Matzler (2005), Surface-based microwave and millimeter wave radiometric remote sensing of the troposphere: A tutorial, *IEEE Geos. Remote Sens. Soc. Newsl.*, *134*, 16–33.

Wood, R. (2005), Drizzle in stratiform boundary layer clouds. Part I: Vertical and horizontal structure, *J. Atmos. Sci.*, *62*, 3011–3033.

Zuidema, P., and K. F. Evans (1998), On the validity of the independent pixel approximation for boundary layer clouds observed during ASTEX, *J. Geophys. Res.*, *103*, 6059–6074.

Zuidema, P., et al. (2005), An Arctic springtime mixed-phase cloudy boundary layer observed during SHEBA, *J. Atmos. Sci.*, *62*, 160–176.

C. Fairall, D. Hazen, and E. R. Westwater, NOAA Environmental Technology Laboratory, R/ET1, 325 Broadway, Boulder, CO 80305, USA.

P. Zuidema, RSMAS/MPO, 4600 Rickenbacker Causeway, Miami, FL 33149-1098, USA. (pzuidema@rsmas.miami.edu)